Characterizing Granular Networks Using Topological Metrics

Joshua Dijksman, Lenka Kovalcinova, Jie Ren, Robert Behringer, Miroslav Kramár, Konstantin Mischaikow, Lou Kondic

▶ To cite this version:

Characterizing Granular Networks Using Topological Metrics

Joshua A. Dijksman,[1] Lenka Kovalcinova*,[2] Jie Ren,[3] Robert P.
Behringer,[4] Miroslav Kramar,[5] Konstantin Mischaikow,[6] and Lou Kondic[2]

[1]*Physical Chemistry and Soft Matter, Wageningen University, Wageningen, The Netherlands*
[2]*Department of Mathematical Sciences, Center for Applied Mathematics and Statistics,*
New Jersey Institute of Technology, Newark, NJ 07102, USA
[3]*Merck Research Laboratories, Merck & Co., Inc., West Point, PA 19486, USA*
[4]*Dept. of Physics, Duke University, Science Drive, Durham NC 27708-0305, USA*
[5]*Advanced Institute for Materials Research, Tohoku University, Sendai, Japan*
[6]*Department of Mathematics, Rutgers University, Piscataway, NJ 08854-8019, USA*

We compare experimental and numerical realizations of a granular system as it undergoes shear jamming. We adjust the numerical methods used to optimally represent the experimental settings. Measures presented here range form microscopic, through mesoscopic to system-wide characteristics of the system. Properties of the mesoscopic force networks provide a key link between micro and macro scales. We report two main findings: the number of particles in the packing that have at least two contacts is a good predictor for the mechanical state of the system, regardless of strain history and packing density. All measures explored in both experiments and numerics, including stress tensor derived measures and contact numbers depend in a universal manner on the fraction of non-rattler particles, f_{NR}. The force network topology also tends to show this universality, yet the shape of the master curve depends much more on the details of the numerical simulations. In particular we show that adding force noise to the numerical data set can significantly alter the topological features in the data. We conclude that both f_{NR} and topological metrics are useful measures to consider when quantifying the state of a granular system.

An important class of particulate systems includes granular materials, colloids, foams and molecular glass formers. These materials can become "rigid", or "jammed", in the absence of long range spatial order. Jammed states are solids in mechanical equilibrium, with non-zero elastic moduli [1, 2]. In order to be in mechanical equilibrium, forces must be transferred from particle to particle, creating self-organized networks of contacts and forces. These networks undergo rearrangements when shear induced deformation of the materials occurs. The networks are typically spatially heterogeneous [3], and during deformation, they are temporally intermittent, with avalanches, slip events, fracture and elasto-plastic failure modes. Finding the microscopic metrics responsible for this broad spectrum of mechanical behaviors across the solid-liquid transition has been challenging, since many of the conventional tools for characterizing ordered thermal systems do not apply.

Understanding how granular materials self-organize into mechanically stable states requires consideration of the structure of force networks. Figure 1 shows examples of typical force networks found in the experiments and simulations. A full description of the force network requires a high dimensional space that reports on microscopic features and does not directly reveal its mesoscopic structure. In order to understand this structure, we need statistical tools for their characterization that are sensitive, systematic, unbiased, minimal, and consistent with macroscopic properties, such as the system-wide stresses. These tools must also be able to distinguish different states of the system, based on force networks.

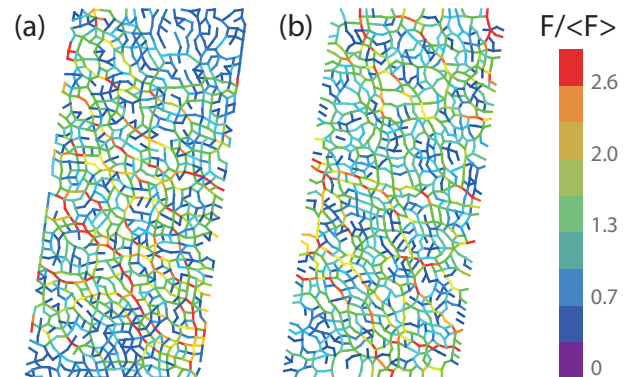To demonstrate the need for mesoscopic description of

FIG. 1. Examples of an experimental (a) and numerical (b) force network. Experimental and numerical examples are generated at the same strain amplitude $\gamma = 14.9\%$ and $\phi = 0.8036$. The color scale represents the total force at each contact, normalized by the concurrent mean force. As described in the text, the simulation results in this and all the following figures include additional noise of amplitude 0.01 N, except if specified differently.

the force network we will consider the granular response to quasi-static shear strain, γ, which is analogous to time in a more conventional dynamical system. The structure of the network as a granular system is strained shows a sensitive dependence on the initial conditions. We show that simple topological measures detect the variability in force networks formed in response to shear in quasi-two-dimensional granular systems. These metrics capture features that are missed by conventional measures,

such as stresses or contact force distributions.

In this article, we consider two realizations of a particular granular system: experimental and computational. The studies of these realizations show the importance of the fraction of non-rattler particles, f_{NR}, defined as particles with at least two contacts, as a relevant state variable. In particular, the considered metrics fall onto master curves when expressed as functions of f_{NR}. These metrics include traditional measures, such as contact numbers, stresses, and contact force probability distribution functions which identify system-wide as well as microscopic features. We observe a good match between the experimental and computational systems at these scales.

However, at the mesoscale, there are clear differences identified using topological metrics. We conjecture that the differences arise from small imperfections and noise in the experiments that are absent in the simulations. The topological metrics that we employ are sensitive to the force noise in the experimental data sets and capture these differences. Our conjecture is reinforced by the fact that by introducing appropriate random noise in the simulations we can generate a reasonable match between the statistics of the topological networks in simulations and experiments. This finding suggests that the considered topological measures may have an important utility in quantifying the properties of intrinsic noise that is always involved in the experiments. As a consequence, topological techniques provide new opportunities for identifying the scale of the experimental noise, and distinguishing noise from intrinsic fluctuations.

Topological metrics Although there exists a number of tools to extract network information, see [4, 5] for reviews, recent work [6–13] demonstrates that topological methods are well suited to characterize force networks in granular packings. In this Letter, we use the Betti numbers β_0 and β_1 to quantify the topology of a network, where β_0 indicates the number of clusters or connected components of the network, and β_1 characterizes the number of loops. Thus, in a rough sense, β_0 is a measure of force network segments, and β_1 is related to their interconnectivity. Computations were performed using software Perseus [14]. In particular, we are interested in the properties of the (simplicial complex) network that describes the force interactions between the particles with force magnitude larger than f_c. We pick $f_c = 1.0\langle|\mathbf{f}|\rangle$ in our analysis (here $\langle|\mathbf{f}|\rangle$ is the average force), and note that results are not very sensitive to this choice of threshold. This network is constructed in the following manner. Every particle, p_i, is represented by a vertex, v_i. The edge $< v_i, v_j >$ belongs to the network if the magnitude of the force interaction, between the corresponding particles p_i and p_j, is larger than f_c. In our construction, we decided to fill in the loops formed by three interacting particles, i.e. we include the triangle $< v_i, v_j, v_k >$ if the pairwise force interactions between the particles exceed f_c. Therefore the boundary of the loops detected by β_1 must contain at least four edges.

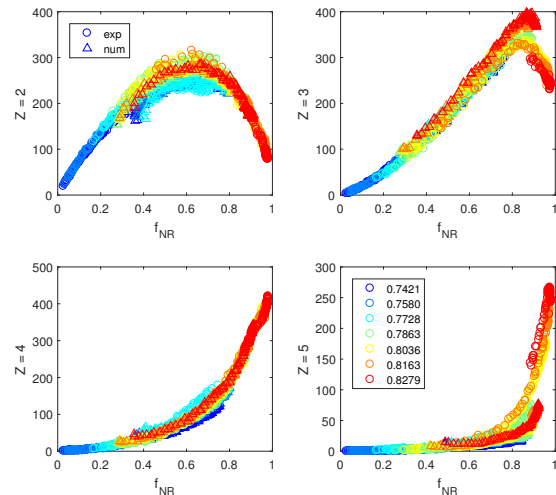While more elaborate tools from algebraic topology

FIG. 2. The evolution of the fraction of particles with contact number $Z_{2,3,4,5}$ as a function of the fraction of non-rattlers f_{NR}, for both experiments (∘) and simulations (△) for a range of ϕ's (color scale). Numerical data color coding has been increased by 0.015 in this and all the following figures as discussed in the text.

have been used to quantify force networks in simulations [15, 16], in the present work we restrict ourselves to the simple measures described above. The reasons for this choice are twofold: *(i)* This method allows for a direct comparison of the statistical properties of force networks between simulations and experiments. To our knowledge, such comparison has not been attempted so far. *(ii)* These methods show potential for assessing the type and size of the noise present in the data [17].

Experimental Details The experiments involve shear of constant-density two dimensional packings of ~ 1000 photoelastic bidisperse disks, starting from a stress free state. The packing density is given in terms of the packing fraction, ϕ. The particles interact via force laws that include friction, and the result is that the applied strain shear-jams the packing [27]. This protocol allows one to probe a large range of mechanically distinct states, from very loose to highly jammed packings. In particular, we use experimental data obtained in a simple shear geometry described in [19, 20] – see the Appendix for details. The particles rest on a co-moving, articulated base, that through its boundaries induces a linear shear profile, suppressing shear bands and other large scale inhomogeneities. We prepare packing fractions from $0.75 \leq \phi \leq 0.825$. We consider results for packings in the range $0.77 \leq \phi \leq 0.825$, where $\phi = 0.77$ is the lowest packing fraction for which we achieve shear jammed states with this apparatus. We then quasi-statically shear the system by a sequence of 100 strain steps of 0.27% each, for a maximum strain of $\gamma = 27\%$ [19], and extract the information about all the forces the particles experience [20]. The force extraction algorithm is applied to each particle

individually. Hence, every contact between two particles yields two force vectors. In the topological analysis we use the average of the norms. Note that this approach has its limitations. First, there exists a lower force threshold below which we cannot detect contacts. By examining the best contact number dynamics match with the numerics for a range of thresholds, we estimate this threshold to be $\approx 0.001N$. Second, for larger pressures, P, we reach a force level such that deformations at contacts become large. We note that the force inverse algorithm assumes small deformations at contacts to make the process more efficient and becomes increasingly inaccurate when $f_{NR} > 0.95$ where deformations are large, so we omit this (small) data set from the analysis where forces are involved. The exact value of this cutoff is not crucial for the present purposes. Furthermore, this is not an intrinsic limitation on the technique; however, since we are mostly interested in behavior near jamming where forces are moderate, amending current algorithms is not necessary.

Simulation Details Despite the simplicity of the numerical scheme, it is highly nontrivial to select the right packing preparation protocol. This sensitivity of granular mechanics to initial preparation is well known even for frictionless systems [21] yet makes a direct comparison between numerical and experimental results very nontrivial. Note that regardless of the preparation protocol chosen, the qualitative behavior observed was always similar; notably the collapse of all data sets as a function of f_{NR} is particularly robust. Two features however required protocol fine tuning: the density *range* and *offset* in which the shear jamming was observed and the network anisotropy. The contact number dynamics and pressure dynamics were not dependent on preparation.

The simulations use a soft-particle non-linear force model and reproduce the experimental settings as closely as possible. The shear geometry, particle sizes and numbers, friction coefficients, density and elastic moduli used in the numerical simulations match the experimental values as taken from the current data or previous work [20, 27]. The inelasticity of the particles is modeled through a coefficient of restitution, frictional interaction between the particles using the Cundall-Strack model [22]. We also simulate a moving base, including translational and rotational friction between the base and the particles. The details of implementation can be found in the Appendix. The simulations reported here are carried out for the same values as for which we have experimental data. We show below that simulations produce results that are comparable to experiments.x

As we will discuss in more detail later, we add random noise to simulation data: all the figures in the paper include this additional noise, unless otherwise specified. Importantly, the essential results shown in Figs. 1 - 3 are insensitive to the noise addition.

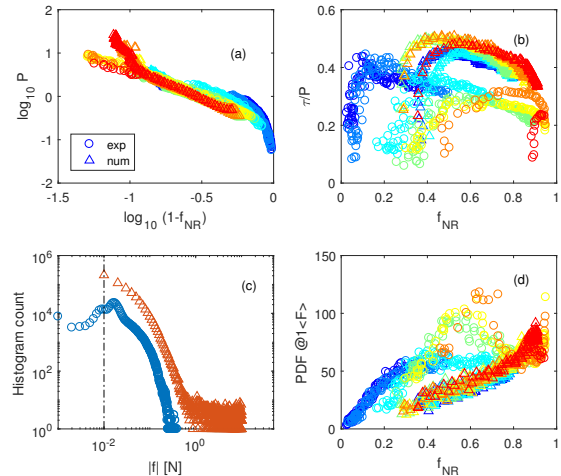*Common features of experiments and simulations* We extract particle positions and inter-particle forces for each particle at every 0.27% strain step, and we compute the local stress tensor $\underline{\sigma}$ using the Irving-Kirkwood method [23]. This provides the pressure from the sum of its eigenvalues $P = (\sigma_1 + \sigma_2)/2$ the shear stress, $\tau = (\sigma_2 - \sigma_1)/2$ and the stress anisotropy, τ/P. At each ϕ, we carry out five realizations in both numerics and experiments, and average the results.

To illustrate the degree of agreement between experiments and simulations when conventional measures are considered, we start by exploring the average number of contacts per particle, Z. This is an important quantity since there is a minimum or isostatic value of Z, Z_{iso} for marginal stability. For frictional particles, $Z_{iso} = N+1$, where N is the system dimension, e.g. $Z_{iso} = 3$ for 2D frictional disks. If a system is sheared from zero stress into a shear jammed state, Z must reach at least $Z_{iso} = 3$ when the system becomes jammed. However, the parts of the force network that first form during the shear jamming process contain a number of particles with only two contacts. Hence, it is relevant to consider not only Z, but also $Z_n(\phi, \gamma)$, the fraction of particles with n contacts.

A key finding in [27] is that many properties such as stresses and Z depend on f_{NR}, in a universal way. Here we show that f_{NR} also determines the dynamics of $Z_n(\phi, \gamma)$. Figure 2 shows data for $Z_{2,3,4,5}$ vs. f_{NR}. There are two outstanding features in this data: *(i)* the dynamics of each Z_n collapses on a single curve, independent of ϕ; and *(ii)* the agreement between experiments and simulations is quantitative. We thus conclude that the simulations reproduce the experiments very well, and that

FIG. 3. (a) Pressure evolution versus 1-f_{NR} for both experiments (○) and simulations (△). (b) Normalized anisotropy τ/P evolution as a function of f_{NR}. (c) histogram of contact force magnitudes $|f|$ for all contacts in the five runs at $\phi = 0.7863$ for both numerics and experiments. The dashed line indicates the force noise added after the numerical runs were completed. (d) The probability distribution function of the norm of the contact forces $P(|\mathbf{f}|)$ as a function of f_{NR} for both experiments (○) and simulations (△) for the force bin centered around $1.2\langle|\mathbf{f}|\rangle$.

f_{NR} can be used as an apparently universal state variable to describe the state of the system.

Figure 3 shows other conventional measures comparing the experimental and the numerical data: in Fig. 3a we see that the experimental pressure data for all ϕ's collapse to a single curve. Furthermore, we find power law scaling for P vs. $1 - f_{NR}$. Intuitively, the inverse relation between P and f_{NR} makes qualitative sense: the larger the fraction of rattlers, $1 - f_{NR}$, the smaller the pressure. However, the power law nature of this relation is not trivial. For the simulations, we also find an excellent collapse of P vs. $1 - f_{NR}$, via a power-law, although the dynamics deviates from power law scaling at large nonrattler fractions, and note a small deviation in the overall pressure scale. A quantitative magnitude agreement in particular in the pressure is sensitive to the choice of inclusion of rattlers, the force law used in the numerics and the area normalization choice in the Irving-Kirkwood formalism, and hence more challenging to get consistent among the experimental and numerical data sets. However, the trends of f_{NR} collapse and $P(f_{NR})$ are mostly insensitive to this.

Figure 3b shows the stress anisotropy, given by τ/P. We find an initial rapid increase of τ from the randomly prepared nominally isotropic stress-free initial state. After this transient, the anisotropy shows only a modest decrease with f_{NR} for both experiments and simulations, while it remains nonzero. The decreasing trend is consistent with the observation that shear jammed states initially have a very anisotropic network, that evolves towards a more isotropic one with increasing strain. The agreement between experiments and simulations is only qualitative, but even though there is modest scatter in the numerical data, the collapse with f_{NR} is obvious.

Force Probability Distribution — A useful microscopic measure is the probability distribution function (PDF) of the norm of the contact forces $P(|\mathbf{f}|)$. Much work has been devoted to characterizing and understanding this distribution [24, 25] although isotropically compressed packings have been the primary focus of past work. Here we examine $P(|\mathbf{f}|)$ vs. f_{NR}, and contrast the experimental $P(|\mathbf{f}|)$ and numerical data. Figure 3c shows the probability of finding a contact force of a certain magnitude in the entire data set at $\phi = 0.7863$. The numerical and experimental histograms are again very similar; the only difference is most likely due to the use of a linear force law in the numerics, where the particles have a much more non-linear interaction. Regardless, the probability distribution function again shows a good collapse with f_{NR}. In Figure 3d we show the bin with force range $1.1 - 1.2\langle|\mathbf{f}|\rangle$. Two features are prominent: First, in both experimental and numerical data, there are good collapses with f_{NR}. Second, experimental and numerical data are in quantitative agreement. The collapse with f_{NR} is observed for other force bins; for example, we have verified that the same feature are observed for force bin centered on $0.5\langle|\mathbf{f}|\rangle$ and $1.5\langle|\mathbf{f}|\rangle$ (see Appendix).

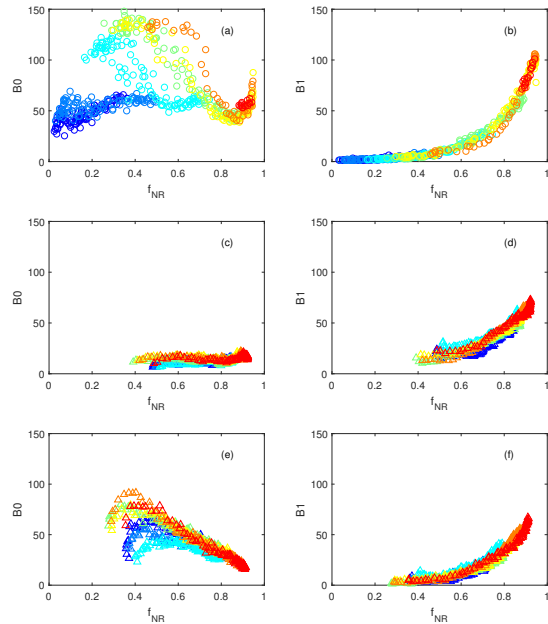The previous metrics have addressed either macro-

FIG. 4. Betti numbers, β_0 (left) and β_1 (right), as a function of f_{NR} for both experiments (a,b: ○) and simulations (c-f, △). (a,b) show original numerical data; (c,d) show the numerical data with 0.01N noise added.

scale or micro-scale structural properties, but do not provide detailed information about the structure of force networks, such as those shown in Fig. 1. We now use topological metrics to analyze the properties of the network that describes the force interactions between the particles with force magnitude larger than $f_c = 1.0\langle|\mathbf{f}|\rangle$.

Figure 4a shows the resulting Betti number dynamics for the experiments. β_0 shows a plateau around 100 and subsequently a decrease. Simulations without added noise (Figure 4c) however, show very different results with much smaller values of β_0: they are essentially independent of f_{NR}. This observation is in a sharp contrast to the findings for more conventional measures, for which experimental and numerical simulations showed at least a qualitative agreement. We see a similar difference in the β_1 dynamics in Figure 4b,d: the numerical data do not seem to asymptote to $\beta_1 = 0$ in the limit of $f_{NR} \to 0$.

The question is: what causes such a dramatic difference in the numerical and experimental network properties? To explain the larger number of the connected components present in the experimental data we propose the following mechanism. Consider the part of the contact network at which the particle interactions are a little below f_c. A slight increase of a single interaction in this region will introduce a new connected component. On the other hand a slight decrease of single interaction, at the region where the interactions are just a little above f_c might result in breaking a connected component into

two pieces. Noise will thus affect topological features in the network. To explore this possibility, we add random noise to the simulations results. The random noise that we use is chosen from a flat distribution within the range of $[0, 0.01]$N that is consistent with the expected level of error in the experiments — see Fig. 3c. Note that after the noise is added to the contact forces, a small force imbalance may result on the particles. The non-zero mean of the added noise is motivated by the fact that we consider here a (positive definite) norm of the force vector.

After noise addition, the agreement between experimental and simulations improves significantly for both β_0 and β_1. Figures 4e shows a monotonically decreasing behavior of β_0, much more in line with experimental data. For β_1 we observe *quantitative* agreement between experiments and simulations. Again, for both β_0 and β_1 we see a good collapse when we consider these quantities as functions of f_{NR}.

Conclusions — In this paper, we have presented one of the first attempts to directly compare microscopic contact force level data from experiments and simulations of dense granular systems. We perform the comparison with metrics across the scales that range from micro to meso and macro. The comparison of micro and macro measures is mostly satisfactory. In particular, we find for both experiments and simulations that, when we express the contact number, pressure, anisotropy, or probability density function of the normal forces as a function of the non-rattler fraction, f_{NR}, we obtain collapse onto master curves, capturing the dynamics over a wide range of conditions.

After finding good agreement for the quantities specified above, it is perhaps surprising to see that the force network in the experiments and simulations, described by Betti numbers, are qualitatively different when raw data from simulations are considered. We argue that contact force noise can be of significant influence on mesoscopic network features, and test this by including adding artificial noise to simulation results. We find that after adding noise of small magnitude, the mesoscopic Betti number dynamics is very similar between experiments and numerics.

On the one hand, the fact that noise influences the properties of force networks, but not classical micro and macro measures listed above is encouraging, since it suggests that the quantities that are commonly observable in granular experiments should not be influenced by typical (experimental) noise. On the other hand, the fact that noise had to be added to simulation results to reach agreement with experiments suggests that direct comparison of the force network properties may be difficult to reach. However, sensitivity of the force networks' properties to noise opens the door towards the use of topological measures to quantify the experimental noise level and its properties, and to distinguish intrinsic fluctuations from experimental noise. Our future work should consider additional measures to provide even better understanding of the properties of force networks and their connection to macroscopic response of particulate-based systems.

Appendix

Methods: Experiments — We discuss here experimental data obtained in a setup described in detail elsewhere [19, 20]. We expose ~ 1000 bi-disperse photoelastic particles in a linear shear cell with articulated bottom. The articulated bottom shear induces linear shear profile, suppressing shear bands other inhomogeneities. We extract the local particle stress by either a nonlinear pattern-fitting algorithm discussed previously [26–28] that yields the complete contact network, particle forces, and stress tensor (e.g. P and τ), or via G^2, the local squared intensity gradient of the photoelastic response, averaged on each particle. G^2 is a one-to-one function of P on the particle level, and provides an easy measure for P. For small data sets, we use the former approach; for larger data sets, we use the latter approach to get only P. In addition to P and τ, we can probe the contact number dynamics with great accuracy: due to the photoelastic response of the disks, we can determine contacts with much more sensitivity than typical distance based metrics [11]. We can thus measure the fraction of particles with n contacts, which we describe with Z_n. We thus also have access to the number of non-rattlers f_{NR}, the particles that are in a force bearing network. Recent work showed [27] showed that this was an important microstructural metric. We probe these structural metrics and force networks in shear jammed states by shearing the system. We prepared packings in a stress free initial state, for $0.75 \leq \phi \leq 0.825$. We then quasi-statically shear the system by 100 small strain steps of 0.27%, up to a total strain of $\gamma = 27\%$ [19]. For the larger ϕ's considered here, we could not apply the full 27% strain because P became so large that the layer of disks was unstable to out-of-plane buckling. If buckling occurs, we terminate the shear experiment. At each packing fraction, we carried out the same shear experiments five times for reproducibility. Beyond a compression level of about 10 N/m or, equivalently, $f_{NR} = 0.95$, the compression of the disks is such that the visibly deform, and hence the force inversion method breaks down. We measure the quality of force extraction by calculating the total image difference between the original photoelastic images and their reconstructed equivalents, where the reconstructed image is based on the fitted contact forces. We show the results in Fig. 7. At large f_{NR} we can clearly see that the image reconstruction becomes significantly different from the image as taken during the experiment, so we omit all data from $f_{NR} > 0.95$.

Methods: Numerics — We perform discrete element simulations using a set of circular disks confined in an initially rectangular domain. The number of the particles ranges from 910 up to 1050, depending on the packing fraction and is set exactly to the number of particles in the experiments. The walls are composed of monodisperse disks. The domain is rectangular, and the length and width of the rectangle are 54 and 27 particle diameters, respectively. System particles are bidisperse and
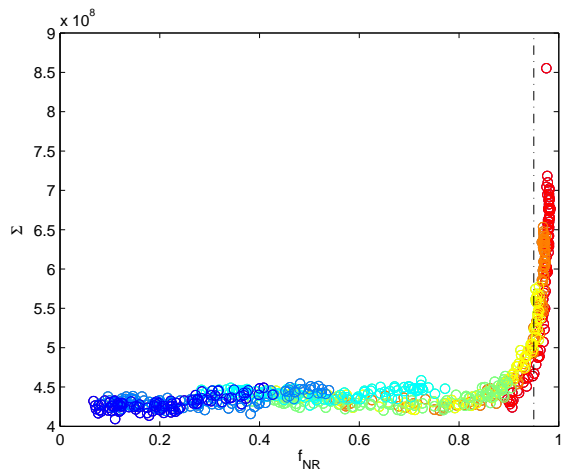
FIG. 5. Integrated image difference Σ for the averaged experimental runs at different densities (color coding, same as main paper). There is a constant background difference due to pixel level noise and other artifacts. The dashed line at $f_{NR} = 0.95$ represents the cutoff we impose in the data selection in the main paper.
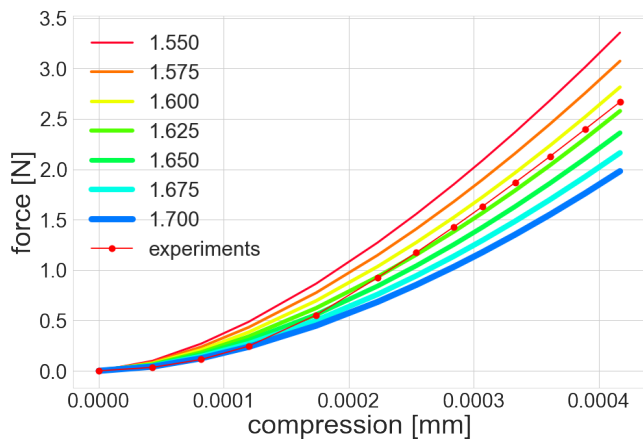

FIG. 6. Calibration curve from experiments (o) and curves using non-linear force model in Equation 1 with different δ.

the ratio of the diameters of the large and small particles is $\approx 15.9/12.7$. The exact positions and particle radii for all packing fractions and different realizations are taken from the initial conditions in the experiments. Particles are soft and interact via normal and tangential forces during collision, with static friction and viscous damping.

The force model used in the simulations is non-lienar; normal force between particles i and j is (see [29] for more details)

$$\mathbf{F}_{i,j}^n = k_n x^\delta \mathbf{n} - \gamma_n x^{0.5} \bar{m} \mathbf{v}_{i,j}^n \qquad (1)$$
$$r_{i,j} = |\mathbf{r}_{i,j}|, \quad \mathbf{r}_{i,j} = \mathbf{r}_i - \mathbf{r}_j, \quad \mathbf{n} = \mathbf{r}_{i,j}/r_{i,j}$$
$$k_n = \frac{2Y}{3(1-\sigma^2)} d_{ave}^{1-\beta}$$

where $1+\beta = \delta$, $\mathbf{v}_{i,j}^n$ is set to the relative normal velocity and Y and σ are Young's modulus and Poisson ratio, respectively. The amount of compression is $x = d_{i,j} - r_{i,j}$, where $d_{i,j} = (d_i + d_j)/2$; d_i and d_j are the diameters of the particles i and j and d_{ave} is the average particle diameter. Here, $\mathbf{r}_i, \mathbf{r}_j$ are the vectors pointing from the centers of particles i, j towards the point of contact.

The exponent δ in the force model is chosen to match the experimental calibration curve measuring the amount of compression of the photoelastic disk particle pressed by a steel plate with a given force. Figure 6 shows the experimental calibration curve and $k_n x^\delta$ curves for chosen values of δ with k_n (dependent on δ, as specified in the set of Equations 1) and $Y = 3.45$ GPa and $\sigma = 0.5$ set to match the experiments. We find that choosing $\delta = 1.625$ yields the least square difference between $k_n x^\delta$ and experimental calibration curve and therefore we use this value of δ in the force model for particle-particle interaction in the simulations.

Here, the characteristic lenghtscale is d_{ave}, the average particle mass, $\bar{m}$, is the mass scale and the binary particle collision time τ_c is the time scale. The value of τ_c is set to [29]

$$\tau_c = \alpha(1+0.5\beta)^{\frac{1}{2+\beta}} \left(\bar{m} \frac{3(1-\sigma^2)}{2Y d_{ave}^{(1-\beta)}} \right)^{\frac{1}{2+\beta}} v_0^{\frac{-\beta}{2+\beta}} \qquad (2)$$

where $v_0 = 0.01423$ ms^{-1} is a characteristic magnitude of velocity in the system (shearing speed); prefactor α and damping coefficient γ_n is obtained as reported in [29].

We implement the commonly used Cundall-Strack model for static friction [22], where a tangential spring is introduced between particles for each new contact that forms at time $t = t_0$. Due to the relative motion of the particles, the spring length, $\boldsymbol{\xi}$, evolves as $\boldsymbol{\xi} = \int_{t_0}^t \mathbf{v}_{i,j}^t (t')\, dt'$, where $\mathbf{v}_{i,j}^t = \mathbf{v}_{i,j} - \mathbf{v}_{i,j}^n$. For long lasting contacts, $\boldsymbol{\xi}$ may not remain parallel to the current tangential direction defined by $\mathbf{t} = \mathbf{v}_{i,j}^t/|\mathbf{v}_{i,j}^t|$ (see, e.g,. [30]); we therefore define the corrected $\boldsymbol{\xi}' = \boldsymbol{\xi} - \mathbf{n}(\mathbf{n} \cdot \boldsymbol{\xi})$ and introduce the test force

$$\mathbf{F}^{t*} = -k_t x^\beta \boldsymbol{\xi}' - \gamma_t x^{0.5} \bar{m} \mathbf{v}_{i,j}^t \qquad (3)$$

where $k_t = 6/7 k_n$ (close to the value used in [31]), γ_t is the coefficient of viscous damping in the tangential direction (with $\gamma_t = \gamma_n$). The value of $\mu = 0.7$ is set to the inter-particle friction from the experiments. To ensure that the magnitude of the tangential force remains below the Coulomb threshold, we constrain the tangential force to be

$$\mathbf{F}^t = min(\mu|\mathbf{F}^n|, |\mathbf{F}^{t*}|)\mathbf{F}^{t*}/|\mathbf{F}^{t*}| \qquad (4)$$

and redefine $\boldsymbol{\xi}$ if appropriate.

In the force model, we include interaction with the base. The force between the particle and the base has a translational and a rotational component and the particle-base friction coefficient is $\mu_b = 0.4$, corresponding to the reported experimental value. The magnitude

of the deceleration of the particle in translational direction due to the friction with base is $\mu_b|\mathbf{g}|$ where $\mathbf{g}$ is the gravitational acceleration. The rotational deceleration of i-th particle due to friction with base

$$|\alpha_i| = \frac{4}{3}\mu_b\frac{|\mathbf{g}|}{r_i} \quad (5)$$

is computed by integrating torque arising from friction with the base and using the moment of inertia of the disk, $I = (m_i r_i^2)/2$, where m_i, r_i are the values of mass and radius of the i-th particle, consecutively. For simplicity, we use $r_i = 1/3 d_{ave}$ for both small and large particles.
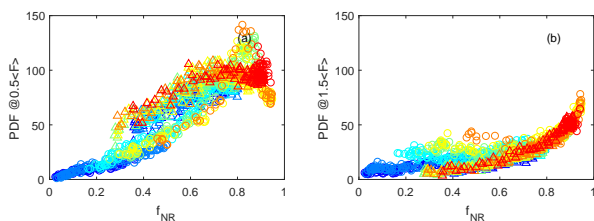

FIG. 7. Probability distribution function of contact forces for a force magnitude bin of $1.2\langle|\mathbf{f}|\rangle$
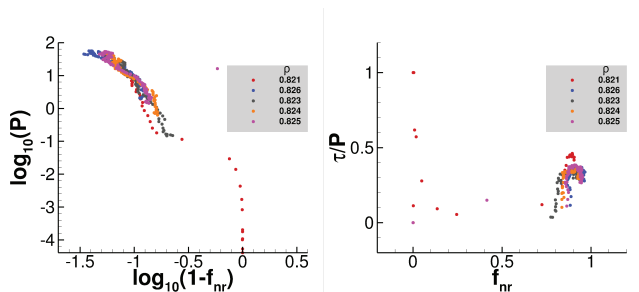

FIG. 8. Pressure, $\log_{10}(P)$ and anisotropy, τ/P as a function of $\log_{10}(1 - f_{nr})$ and f_{nr}, respectively.

We integrate Newton's equations of motion for both the translation and rotational degrees of freedom using

a 4th order predictor-corrector method with time step $\Delta t = 0.02\tau_c$.

From the initial configuration taken from the experiments, the system is sheared by moving the left wall in positive and the right wall in the negative direction. Shearing speed used in the simulations, expressed in the units of d_{ave}/τ_c, is $v_0' = 2.5 \times 10^{-5}$. Relaxation is interjected after each strain step of 0.27%. The maximum strain amplitude is 27%.

Consistency checks —

In this section we present consistency checks; specifically, we focus on the distribution of the forces measured in both experiments and simulations for a different force bin than in the main body of the paper. Then we show that the particle-particle and particle-base friction is essential if we want to achieve a quantitative agreement between simulations and experiments.

In Figure 3d we show the probability distribution function of contact forces for a force magnitude bin of $1.2\langle|\mathbf{f}|\rangle$. In Figure 7 we show that the f_{NR} collapse and consistency between experimental and numerical data is retained for the force bin around $0.5\langle|\mathbf{f}|\rangle$ (a) and $1.5\langle|\mathbf{f}|\rangle$ (b). Thus we conclude that our results comparing force distribution is not sensitive to the choice of the bin.

To demonstrate the importance of having a non-zero friction coefficient, we consider the dynamics of pressure and anisotropy for a few single runs with $\mu = 0.0$ and $\mu_b = 0.0$ at various packing fractions around the jamming point as observed in our protocol. Figure 8 shows P and τ/P as a function of f_{nr} for frictionless systems. Evidently, our numerical protocol does not produce the same f_{NR} dynamics as the experiments, even though the pressure and anisotropy values remain within a similar range in jammed systems (especially for large f_{NR}).

[1] A. J. Liu and S. R. Nagel, Nature **396** 21-22 (1998).
[2] M. van Hecke, J. Phys. Cond. Matt. **22** 033101 (2010).
[3] B. Cambou, M. Jean and F. Radjai (eds.), Micromechanics of Granular Materials (Wiley, 2009).
[4] R. Albert and A.L. Barabasi, Rev. Mod. Phys. 74, 47 (2002).
[5] S. Alexander, Phys. Rep. 296, 65 (1998).
[6] D.S. Bassett, E.T. Owens, K. E. Daniels and M.A. Porter, *Phys. Rev. E* **86**, 041306 (2012)
[7] J.P. Peters, M. Muthuswamy, J. Wibowo and A. Tordesillas, *Phys. Rev. E* **72**, 041307 (2005)
[8] A. Tordesillas, D. M. Walker and Q. Lin, *Phys. Rev. E* **81** 011302 (2010)
[9] G. Carlsson, J. Gorham, M. Kahle, J. Mason, Phys. Rev. E, **85**, 011303 (2012).
[10] R. Arevalo, I. Zuriguel, L. A. Pugnaloni and D. Maza, Phys. Rev. E, **87**, 022203 (2013).
[11] S. Ardanza-Trevijano, I. Zuriguel, R. Arevalo and D.

Maza, Phys. Rev. E, **89**, 052212 (2014).

[12] L. Kondic et al, *EPL* **97** 54001 (2012)

[13] M. Kramar, A. Goullet, L. Kondic, and K. Mischaikow, *Phys. Rev. E* **87**, 042207 (2013).

[14] K. Mischaikow and V. Nanda, *Disc. & Comp. Geom.* **50** 330 (2013).

[15] L.A. Pugnaloni, C. M. Carlevaro, M. Kramár, K. Mischaikow and L. Kondic, *Phys. Rev. E* **93** 062902 (2016)

[16] L. Kondic, M. Kramár, L. A. Pugnaloni, C. M. Carlevaro and Mischaikow, K., *Phys. Rev. E*, **93**, 062903 (2016)

[17] O. Bobrowski, M. Kahle, To appear in: *Topology in Statistical Inference, the Proceedings of Symposia in Applied Mathematics; arXiv* 1409.4734 (2014) .

[18] D. Bi, J. Zhang, B. Chakraborty and R. P. Behringer, Nature **480** 355-358 (2011).

[19] J. Ren, J. A. Dijksman, and R. P. Behringer, Chaos **21** 041105 (2011) and at the online image gallery, American Physical Society, Topical Group on Statistical and Nonlinear Physics (2011)

[20] J. Ren, J.A. Dijksman, R. P. Behringer, *Phys. Rev. Lett.* **110** 018302 (2013).

[21] C. P. Goodrich, S. Dagois-Bohy, B. P. Tighe, M. van Hecke, A. J. Liu, and S. R. Nagel, *Phys. Rev. E* **90**, 022138 (2014)

[22] P.A. Cundall and O.D.L. Strack. *Géotechnique* **29** 4765 (1979).

[23] J. H. Irving and J. G. Kirkwood. *J. Chem. Phys.* **18** 817 (1950).

[24] B. P. Tighe and T. J. H. Vlugt, *J. Stat. Mech.* **2011** P04002 (2011).

[25] E. I. Corwin, H. M. Jaeger and S. R. Nagel, *Nature* **435** 1075-1078 (2005)

[26] J. Zhang, T. Majmudar, A. Tordesillas, and R. P. Behringer, Granular Matter **12** 159-172 (2010).

[27] D. Bi, J. Zhang, B. Chakraborty and R. P. Behringer, Nature **480** 355-358 (2011).

[28] T. S. Majmudar, M. Sperl, S. Luding and R. P. Behringer, *Phys. Rev. Lett.* **98**, 058001 (2007).

[29] Kondic L. Dynamics of spherical particles on a surface: Collision-induced sliding and other effects. *Phys. Rev. E*, **60** 751 (1999).

[30] Brendel L. and Dippel S. in *Physics of Dry Granular Media*, edited by Herrmann H. J., Hovi J.-P. and Luding S. (Kluwer Academic Publishers, Dordrecht, 1998).

[31] Goldenberg C., Goldhirsch I. Friction enhances elasticity in granular solids. *Nature*, **435** 188 (2005).